



## Article

# Crystal Chemistry, Thermal and Radiation-Induced Conversions and Indicatory Significance of S-Bearing Groups in Balliranoite

Nikita V. Chukanov <sup>1,2,\*</sup>, Anatoly N. Sapozhnikov <sup>3</sup>, Roman Yu. Shendrik <sup>2,3</sup> , Natalia V. Zubkova <sup>2</sup>, Marina F. Vigasina <sup>2</sup> , Nadezhda V. Potekhina <sup>2</sup>, Dmitry A. Ksenofontov <sup>2</sup> and Igor V. Pekov <sup>2</sup>

- <sup>1</sup> Federal Research Center of Problems of Chemical Physics and Medicinal Chemistry, Russian Academy of Sciences, 142432 Chernogolovka, Moscow Region, Russia
- <sup>2</sup> Faculty of Geology, Moscow State University, 119991 Moscow, Russia; roshen@yandex.ru (R.Y.S.); n.v.zubkova@gmail.com (N.V.Z.); vigasina55@mail.ru (M.F.V.); estel58@yandex.ru (N.V.P.); ksen53@gmail.com (D.A.K.); igorpekov@mail.ru (I.V.P.)
- <sup>3</sup> Vinogradov Institute of Geochemistry, Siberian Branch of Russian Academy of Sciences, 664033 Irkutsk, Russia; sapozh@igc.irk.ru
- \* Correspondence: chukanov@icp.ac.ru

**Abstract:** Crystal-chemical features of a sulfide-bearing variety of the cancrinite-group mineral balliranoite from the Tuluyskoe lapis lazuli deposit, Baikal Lake area, Siberia, Russia, have been investigated using a multimethodic approach based on infrared (IR), Raman, and electron spin resonance (ESR), as well as ultraviolet, visible and near infrared (UV–Vis–near IR) absorption spectroscopy methods, luminescence spectroscopy, electron microprobe analysis, selective sorption of CO<sub>2</sub> and H<sub>2</sub>O from annealing products, and single-crystal X-ray structure analysis. Holotype balliranoite and its sulfate analogue, davyne, were studied for comparison. The crystal-chemical formula of the studied sample from Tultuyskoe is Na<sub>5.4</sub>K<sub>0.1</sub>Ca<sub>2.4</sub>(Si<sub>6</sub>Al<sub>6</sub>O<sub>24</sub>)Cl<sub>2</sub>[(CO<sub>3</sub>)<sub>0.7</sub>(SO<sub>4</sub>)<sub>0.18</sub>S\*<sub>0.95</sub>Cl<sub>0.1</sub>(H<sub>2</sub>O)<sub>0.16</sub>], where the content of the wide zeolite channel is given in square brackets; S\* is total sulfide sulfur occurring as disordered S<sub>2</sub><sup>•−</sup>, *cis*- and *trans*-S<sub>4</sub>, S<sub>5</sub><sup>2−</sup>, minor S<sub>3</sub><sup>•−</sup>, and HS<sup>−</sup> groups. The presence of S<sub>5</sub><sup>2−</sup> and HS<sup>−</sup> groups, the absence of CO<sub>2</sub> molecules, and the association with pyrrhotite and Fe-free pargasite indicate that the studied sample crystallized under highly reducing, low-temperature conditions, unlike holotype balliranoite whose formation was related to the Somma-Vesuvius volcanic complex, Italy. Irradiation of balliranoite from Tultuyskoe with X-rays results in the transformations of polysulfide groups other than S<sub>3</sub><sup>•−</sup> into S<sub>3</sub><sup>•−</sup> in accordance with the scheme: S<sub>5</sub><sup>2−</sup> → S<sub>2</sub><sup>•−</sup> + S<sub>3</sub><sup>•−</sup>; 3S<sub>2</sub><sup>•−</sup> → 2S<sub>3</sub><sup>•−</sup> + e<sup>−</sup>; S<sub>4</sub> + S<sub>2</sub><sup>•−</sup> + e<sup>−</sup> → 2S<sub>3</sub><sup>•−</sup>; S<sub>4</sub> + S<sub>2</sub><sup>•−</sup> + e<sup>−</sup> → 2S<sub>3</sub><sup>•−</sup>; S<sub>4</sub> + S<sub>5</sub><sup>2−</sup> + e<sup>−</sup> → 3S<sub>3</sub><sup>•−</sup> (e<sup>−</sup> = electron).

**Keywords:** balliranoite; cancrinite group; isomorphism; sulfur; polysulfide groups; infrared spectroscopy; electron spectroscopy; Raman spectroscopy; electron spin resonance; photoluminescence; X-ray structural analysis; Tultuyskoe lapis lazuli deposit



**Citation:** Chukanov, N.V.; Sapozhnikov, A.N.; Shendrik, R.Y.; Zubkova, N.V.; Vigasina, M.F.; Potekhina, N.V.; Ksenofontov, D.A.; Pekov, I.V. Crystal Chemistry, Thermal and Radiation-Induced Conversions and Indicatory Significance of S-Bearing Groups in Balliranoite. *Minerals* **2023**, *13*, 822. <https://doi.org/10.3390/min13060822>

Academic Editor: Lidong Dai

Received: 30 May 2023

Revised: 14 June 2023

Accepted: 14 June 2023

Published: 16 June 2023



**Copyright:** © 2023 by the authors. Licensee MDPI, Basel, Switzerland. This article is an open access article distributed under the terms and conditions of the Creative Commons Attribution (CC BY) license (<https://creativecommons.org/licenses/by/4.0/>).

## 1. Introduction

Various extra-framework anions, radical anions, and neutral molecules (SO<sub>4</sub><sup>2−</sup>, SO<sub>3</sub><sup>2−</sup>, PO<sub>4</sub><sup>3−</sup>, CO<sub>3</sub><sup>2−</sup>, C<sub>2</sub>O<sub>4</sub><sup>2−</sup>, Cl<sup>−</sup>, HS<sup>−</sup>, OH<sup>−</sup>, F<sup>−</sup>, S<sub>n</sub><sup>2−</sup> with *n* from 1 to 5, S<sup>•*n*−</sup> with *n* from 1 to 4, where “•” means unpaired electron, S<sub>n</sub><sup>0</sup> with *n* = 4 or 6, CO<sub>2</sub>, COS, and H<sub>2</sub>O) occurring in cancrinite- and sodalite-group minerals [1–14] are considered as important markers of redox conditions and fugacities of volatile components during rock formation [14–17]. The S-bearing extra-framework species are most diverse and indicate wide variations of the oxidation degree of sulfur, polymerization degree of sulfide sulfur, and charges of S-bearing species. Unlike the majority of minerals of the cancrinite and sodalite groups from volcanic complexes, their counterparts from metasomatic lapis lazuli deposits contain sulfur

in both oxidized (sulfate,  $\text{SO}_4^{2-}$ ) and reduced (mainly, polysulfide, rarely monosulfide,  $\text{S}^{2-}$ , as well as  $\text{HS}^-$ , or sulfite,  $\text{SO}_3^{2-}$ ) forms, which reflects reducing conditions of their formation [4–6,9,12–14,17,18].

Balliranoite, ideally  $(\text{Na,K})_6\text{Ca}_2(\text{Si}_6\text{Al}_6\text{O}_{24})\text{Cl}_2(\text{CO}_3)$ , is a rare cancrinite-group mineral first discovered at the Somma-Vesuvius volcanic complex, Campania, Italy [19]. This mineral forms a solid-solution series with davyne,  $(\text{Na,K})_6\text{Ca}_2(\text{Si}_6\text{Al}_6\text{O}_{24})\text{Cl}_2(\text{SO}_4)$  [20,21]. Structurally, both minerals are closely related to cancrinite,  $\text{Na}_7\text{Ca}[\text{Al}_6\text{Si}_6\text{O}_{24}](\text{CO}_3)_{1.5}\cdot 2\text{H}_2\text{O}$ , and vishnevitte,  $(\text{Na,K})_8[\text{Al}_6\text{Si}_6\text{O}_{24}](\text{SO}_4)\cdot 2\text{H}_2\text{O}$  [22–24], as well as their high-chloride analogue, betzite,  $\text{Na}_6\text{Ca}_2(\text{Al}_6\text{Si}_6\text{O}_{24})\text{Cl}_4$ , recently discovered in a xenolith hosted by alkaline basalt of the *Bellerberg paleovolcano*, Eifel Mountains, Germany [25]. The aluminosilicate frameworks of balliranoite, davyne, and betzite contain columns of cancrinite cages hosting  $(\text{Ca}\cdots\text{Cl})_\infty$  chains and wide channels which contain the  $\text{CO}_3^{2-}$ ,  $\text{SO}_4^{2-}$ , and  $\text{Cl}^-$  anions, as well as extra-framework cations ( $\text{Na}^+$ ,  $\text{K}^+$ , and minor  $\text{Ca}^{2+}$ ). Columns of cancrinite cages of other minerals with the cancrinite-type aluminosilicate frameworks host  $(\text{Na}\cdots\text{H}_2\text{O})_\infty$  chains. Based on the content of the columns of cancrinite cages, the two-layer cancrinite-group minerals can be subdivided into the subgroup of cancrinite *sensu stricto* and the davyne subgroup [26]. Unlike balliranoite, davyne and intermediate members of the balliranoite-davyne solid-solution series are rather widespread minerals known in numerous localities [1,20,22,27–30].

The rarity of balliranoite may be caused by the combination of two extra-framework anions which are characteristic for cancrinite-group members from different geological environments:  $\text{CO}_3^{2-}$ , occurring in wide channels, is typical for the minerals formed in intrusive complexes, whereas  $\text{Cl}^-$  is more common for cancrinite-group minerals from volcanic complexes [24]. However, there is a specific formation, the skarn-like lazurite-bearing metasomatites related to relatively abyssal rocks, in which cancrinite-group minerals demonstrate crystal-chemical features rather similar to those from low-pressure volcanic rocks. This paper describes crystal-chemical features of an unusual sulfide-bearing variety of balliranoite from the Tultuyskoe lapis lazuli deposit (Baikal Lake area, Siberia, Russia) belonging to this formation. The application of a multimethodic approach based on infrared (IR) absorption; Raman; electron spin resonance (ESR); ultraviolet, visible, and near infrared (UV–Vis–NIR) absorption spectroscopy; spectroscopy of luminescence; electron microprobe analysis; selective sorption of  $\text{CO}_2$  and  $\text{H}_2\text{O}$  from annealing products; and single-crystal X-ray structure analysis made it possible to identify ten (!) extra-framework components occurring in this sample. Additionally, radiation-induced and thermal transformations of sulfide-bearing balliranoite were studied.

## 2. Materials and Methods

### 2.1. Samples

Three samples were studied. The most detailed data have been obtained for sulfide-bearing balliranoite (below, Sample 1) from the abandoned Tultuyskoe (another name: Tultuy, or Tultui) lapis lazuli deposit situated in the valley of Tultuy, a left tributary of the Malaya Bystraya river, Baikal Lake area, Siberia, Russia. The Tultuyskoe deposit was discovered in 1852 by G. M. Permikin. Its specific feature distinguishing it from other lapis lazuli occurrences of the Baikal Lake area is the abundance of cancrinite-group minerals (mainly, afghanite, with the subordinate roles of tounkite and balliranoite) as well as the sodalite-group member vladimirivanovite, an orthorhombic analogue of minerals belonging to the lazurite–häuyne solid-solution series [21].

**Sample 1** contains light green to greenish yellow grains of sulfide-bearing balliranoite embedded in granular calcite aggregates up to 2 cm across (Figure 1). These aggregates occur in calcite marble containing accessory pyrrhotite, amphibole, and dolomite. Other minerals closely associated with sulfide-bearing balliranoite are fluorapatite, sodalite, and pargasite.



**Figure 1.** Balliranoite (green to greenish yellow, in calcite) from Tultuyskoe (Sample 1). Field of view width: 7 mm.

Samples 2 and 3 were studied for comparison. These samples were partly characterized by us earlier [19,29].

**Sample 2** is the holotype specimen of balliranoite from the Somma-Vesuvio volcanic complex [19]. It occurs as colorless equant and prismatic crystals up to  $1\text{ mm} \times 1\text{ mm} \times 2\text{ mm}$  (Figure 2) in cavities of metasomatic rock composed of orthoclase, phlogopite, clinohumite, calcite, diopside, pargasite, haüyne, and fluorapatite. The empirical formula of balliranoite from Sample 2 is  $\text{Na}_{4.70}\text{Ca}_{2.53}\text{K}_{0.73}(\text{Si}_{6.02}\text{Al}_{5.98}\text{O}_{23.995})\text{Cl}_{2.34}(\text{CO}_3)_{0.82}(\text{SO}_4)_{0.27} \cdot 0.12\text{H}_2\text{O}$ . It is hexagonal, space group  $P6_3$ ;  $a = 12.695(2)\text{ \AA}$ ,  $c = 5.325(1)\text{ \AA}$ ,  $V = 743.2(2)\text{ \AA}^3$ , and  $Z = 1$ .



**Figure 2.** Crystals of balliranoite from the Somma-Vesuvio volcanic complex (Sample 2). Field of view width: 1 mm.

**Sample 3** is davyne from Sar'e Sang, the famous lapis lazuli deposit in Afghanistan. It forms light blue aggregates in association with lazurite, diopside, and calcite (Figure 3). Its empirical formula is  $\text{Na}_{5.1}\text{Ca}_{2.0}\text{K}_{0.8}(\text{Si}_{6.0}\text{Al}_{6.0}\text{O}_{24})\text{Cl}_{2.0}(\text{SO}_4)_{0.9}(\text{S}_2^{\bullet-})_{0.1}$  and parameters of the unit cell are  $a = 12.773(1)$ ,  $c = 5.334(1)$  Å; space group  $P6_3$  [29].



**Figure 3.** Davyne (light blue) in association with lazurite (dark blue), diopside (yellowish grey) and calcite (white) from Sar'e Sang (Sample 3). Field of view width: 18 mm.

## 2.2. Analytical Methods

In order to obtain IR absorption spectra, powdered samples were mixed with anhydrous KBr, pelletized, and analyzed using an ALPHA FTIR spectrometer (Bruker Optics, Karlsruhe, Germany) at a resolution of  $4\text{ cm}^{-1}$  as described in [5,6,8,12,13]. A total of 16 scans were collected for each spectrum. The IR spectrum of an analogous pellet of pure KBr was used as a reference.

The Raman spectra have been obtained for randomly oriented grains using an EnSpectr R532 spectrometer based on an OLYMPUS CX 41 microscope (Enhanced Spectrometry, San Jose, CA, USA) coupled with a diode laser ( $\lambda = 532\text{ nm}$ ) at room temperature [5,8,12,15]. The spectra were recorded in the range from  $100$  to  $4000\text{ cm}^{-1}$  with a diffraction grating ( $1800\text{ gr mm}^{-1}$ ) and spectral resolution of about  $6\text{ cm}^{-1}$ . The output power of the laser beam was in the range from 15 to 20 mW. The diameter of the focal spot on the sample was 5–20  $\mu\text{m}$ . The backscattered Raman signal was collected with  $10\times$  and  $40\times$  objectives; signal acquisition time for a single scan of the spectral range was 1 s, and the signal was averaged over 100 scans. Crystalline silicon was used as a standard.

The assignment of bands in the IR and Raman spectra was carried out using data from [5–9,12–16,18,31–34].

The absorption spectra of a 1.1 mm thick fragment of Sample 1 in the UV–Vis–NIR range were measured at room temperature using a Lambda 950 spectrophotometer (Perkin-Elmer, Shelton, CT, USA) as described in [12,13].

Irradiation of Sample 1 was carried out with a low-pressure mercury lamp at room temperature for 30 min from both sides. X-ray irradiation was carried out at room temperature using an X-ray tube with a Pd anode with an applied voltage of 25 kV and a current of 20 mA.

ESR spectra of Sample 1 were measured on a randomly oriented grain with a RE-1306 X-band spectrometer (KBST, Smolensk, Russia) at room temperature and at 77 K as described in [12,15]. For low-temperature measurements, a quartz ampoule with the sample was placed in a flooded nitrogen quartz cryostat.

The luminescence excitation spectra were measured on an LS-55 spectrofluorometer (Perkin-Elmer, Shelton, CT, USA) in a cryostat at a temperature of 77 K. The luminescence spectra were measured on a spectrometer based on an MDR-2 monochromator (LOMO, Saint-Petersburg, Russia) using a diffraction grating with 600 lines per millimeter, upon excitation with a 405 nm semiconductor laser. The spectra registration was carried out using a Hamamatsu H10721-04 photomodule (Hamamatsu, Sendai, Japan).

The single-crystal XRD studies were carried out using an Xcalibur S diffractometer (OXFORD DIFFRACTION, Oxford, UK) equipped with a CCD detector (MoK $\alpha$  radiation,  $\lambda = 0.71073$  Å), operating at 50 kV and 40 mA. More than a hemisphere of three-dimensional data was collected at room temperature from the crystal of  $0.35 \times 0.54 \times 0.82$  mm<sup>3</sup> in size. Data reduction was performed using the CrysAlisPro Version 1.171.37.35 [35]. The data were corrected for Lorentz factor and polarization effects.

Five EDS-mode electron microprobe analyses of Sample 1 were carried out on an analytical suite including a digital scanning electron microscope Tescan VEGA-II XMU equipped with an energy-dispersive spectrometer (EDS) INCA Energy 450 with semi-conducting Si (Li) detector Link INCA Energy and wave-dispersive spectrometer (WDS) Oxford INCA Wave 700, produced by Tescan Orsay Hld., Brno, Czech Republic. The analyses were performed at an accelerating voltage of 20 kV, current of 120 to 150 pA, and beam diameter of 120 nm. The diameter of the excitation zone was below 5  $\mu$ m. The following standards were used: albite for Na, potassium feldspar for K, wollastonite for Ca, synthetic Al<sub>2</sub>O<sub>3</sub> for Al, SiO<sub>2</sub> for Si, FeS<sub>2</sub> for S, and NaCl for Cl. Contents of other elements with atomic numbers > 6 are below detection limits.

The H<sub>2</sub>O content was determined by means of the Penfield method. In order to determine the content of carbonate groups, selective sorption of CO<sub>2</sub> was carried out on *askarite* sorbent (an asbestiform matter saturated by NaOH) from gaseous products obtained by heating of the mineral at 1080 °C in oxygen at 1 atm.

### 3. Results

#### 3.1. Chemical Composition

The chemical composition of sulfide-bearing balliranoite (Sample 1) is given in Table 1. Chemically, the mineral is quite uniform. Significant variations are observed only for the contents of calcium and sulfur. Oxygen equivalent for polysulfide groups is not calculated because they are disordered and their proportion could not be determined based on X-ray structural data. However, the total sums of analyses significantly exceeding 100% indicate that a major part of sulfur occurs in polysulfide groups. This conclusion was qualitatively confirmed by a combination of spectroscopic methods (see below). In order to subtract oxygen equivalents, exact contents of different polysulfide groups are required. Unfortunately, application of a complex of spectroscopic methods provides only qualitative information on the contents of these groups.

The empirical formula of Sample 1 based on 12 (Si + Al) atoms per formula unit is H<sub>0.33</sub>Na<sub>5.31</sub>K<sub>0.13</sub>Ca<sub>2.59</sub>(Al<sub>6.00</sub>Si<sub>6.00</sub>O<sub>24</sub>)S\*<sub>1.13</sub>O<sub>y</sub>(CO<sub>3</sub>)<sub>0.69</sub>Cl<sub>2.09</sub>, where S\* is total sulfur and O<sub>y</sub> is oxygen belonging to sulfate groups and H<sub>2</sub>O molecules.

**Table 1.** Chemical composition (wt.%) of sulfide-bearing balliranoite (Sample 1).

Component	Spot Analysis No.					Mean
	1	2	3	4	5	
Na <sub>2</sub> O	15.00	15.09	14.90	14.79	14.95	14.95
K <sub>2</sub> O	0.78	0.51	0.51	0.37	0.59	0.55
CaO	12.81	12.84	12.86	13.91	13.47	13.17
Al <sub>2</sub> O <sub>3</sub>	27.17	28.04	27.87	28.00	27.65	27.75
SiO <sub>2</sub>	33.11	32.55	32.54	32.82	32.65	32.73
SO <sub>3</sub>	8.32	8.83	8.86	7.34	7.78	8.23
Cl	6.65	6.73	6.75	6.57	6.94	6.73
−O≡Cl	−1.50	−1.52	−1.52	−1.48	−1.57	−1.52
CO <sub>2</sub>	-	-	-	-	-	2.75
H <sub>2</sub> O	-	-	-	-	-	0.27
Total	102.34	103.07	102.77	102.32	102.46	105.61

Note: All sulfur is given as SO<sub>3</sub>.

### 3.2. Infrared Spectroscopy

The IR spectra of the studied samples are given in Figure 4. They contain bands of stretching (in the range of 950–1130 cm<sup>−1</sup>), mixed (550–700 cm<sup>−1</sup>), and bending (below 500 cm<sup>−1</sup>) vibrations of the aluminosilicate framework, partly overlapping with weaker bands of stretching and bending modes of sulfate anions (in the ranges of 1100–1200 and 610–620 cm<sup>−1</sup>, respectively). Bands at 3300 to 3368 cm<sup>−1</sup> correspond to O–H stretching vibrations of H<sub>2</sub>O molecules. Weak bands in the range from 710 to 780 cm<sup>−1</sup> may be due to combination modes [25].

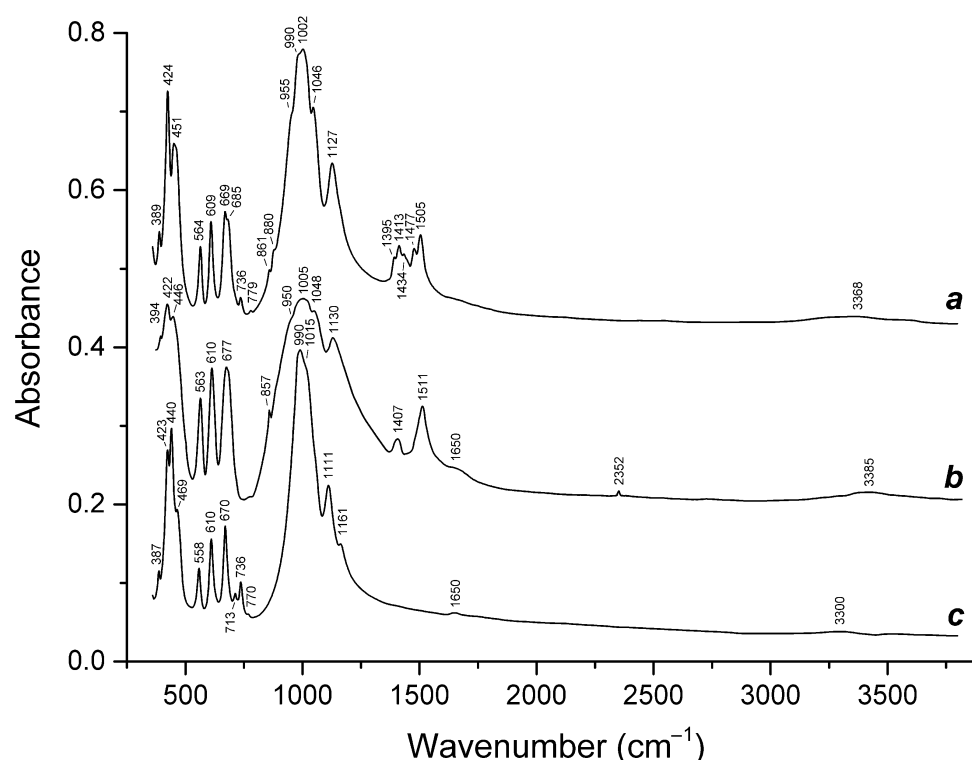


**Figure 4.** IR spectra of (a) balliranoite from Tultuyskoe (Sample 1), (b) holotype balliranoite (Sample 2) and (c) davyne (Sample 3).

IR spectra of both balliranoite samples differ from that of davyne by the presence of additional bands of asymmetric stretching and out-of-plane bending modes of CO<sub>3</sub><sup>2−</sup> groups (in the ranges of 1390–1520 and 850–880 cm<sup>−1</sup>, respectively). As compared to holotype balliranoite, Sample 1 shows additional bands of CO<sub>3</sub><sup>2−</sup> groups at 880, 1395,

1434 and 1477  $\text{cm}^{-1}$ , which indicates the presence of carbonate groups in a different local environment. The shoulder at 685  $\text{cm}^{-1}$  may correspond to *trans*- $\text{S}_4$  symmetric stretching  $\nu_3$  mode.

In the IR spectrum of holotype balliranoite (Sample 2), bands of framework stretching and bending bands are poorly resolved, which may be due to the presence of  $\text{Fe}^{3+}$  defects in the framework which were detected with luminescence (see below), or a partial disordering of Si and Al. The peak at 2352  $\text{cm}^{-1}$  corresponds to antisymmetric stretching vibrations of  $\text{CO}_2$  molecules occurring in the channel.

### 3.3. Raman Spectroscopy

Unlike IR spectroscopy, Raman spectroscopy is very sensitive to the presence of different species containing sulfide sulfur. However, the application of Raman spectroscopy can be complicated by luminescence. Figure 5 shows uncorrected Raman spectra of the studied samples. Strong luminescence is observed as a combination of at least three very broad peaks centered in the ranges of 1500–2000, 2700–3100 and 3300–3600  $\text{cm}^{-1}$  which may be due to the presence of  $\text{Mn}^{2+}$ ,  $\text{S}_2^{\bullet-}$  and  $\text{Fe}^{3+}$  centers, respectively [5,14,15,36].

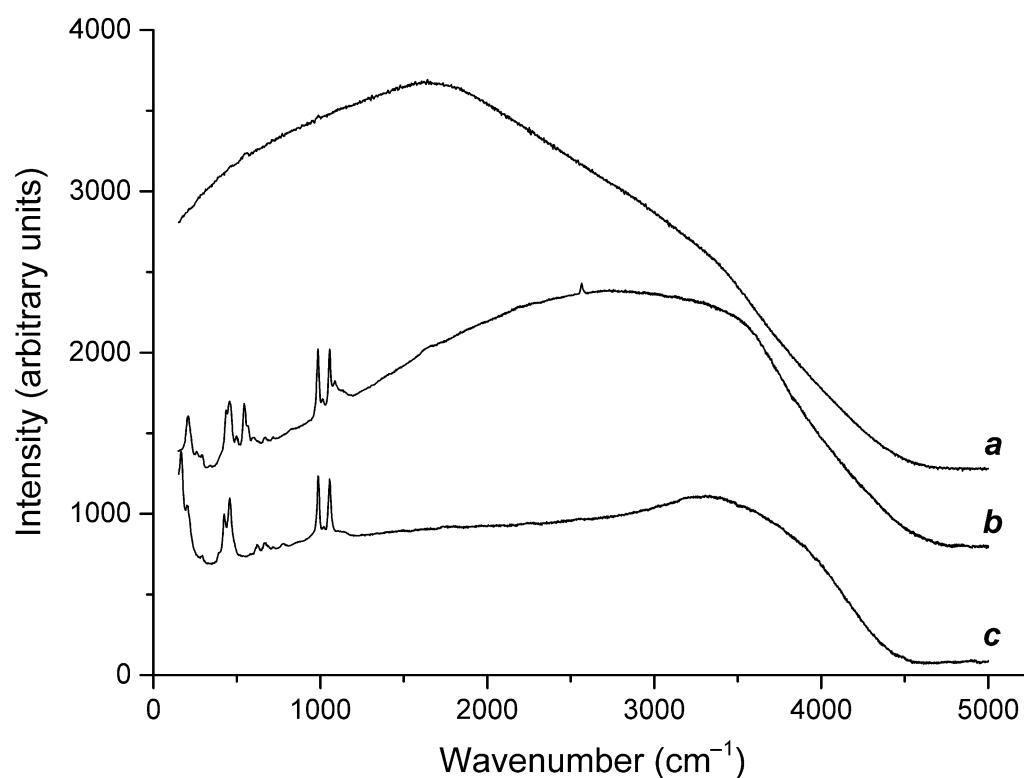


**Figure 5.** Uncorrected Raman spectra of (a) davyne (Sample 3), (b) balliranoite from Tultuy (Sample 1) and (c) holotype balliranoite (Sample 2) showing strong fluorescence.

The Raman spectrum of balliranoite from Tulyui in the range of 1200–3800  $\text{cm}^{-1}$  contains weak bands at ~1640 and 2564  $\text{cm}^{-1}$  corresponding to  $\text{S}_3^{\bullet-}$  overtone ( $3\nu_1$ ) and  $\text{HS}^-$  stretching mode, respectively [6–8,12,15].

Corrected Raman spectra of balliranoite (the Samples 1 and 2) in the range of 150–1250  $\text{cm}^{-1}$  are shown in Figure 6. In the Raman spectrum of holotype balliranoite, only bands of  $\text{CO}_3^{2-}$ ,  $\text{SO}_4^{2-}$ , and aluminosilicate framework are observed (Table 2). The Raman spectrum of balliranoite from Tultuyskoe contains in this region additional bands of  $\text{S}_2^{\bullet-}$ ,  $\text{S}_3^{\bullet-}$ , *cis*- $\text{S}_4$ , *trans*- $\text{S}_4$ , and  $\text{S}_5^{2-}$ . Their assignment made using data from [5–9,12–16,18–22] is given in Table 2.

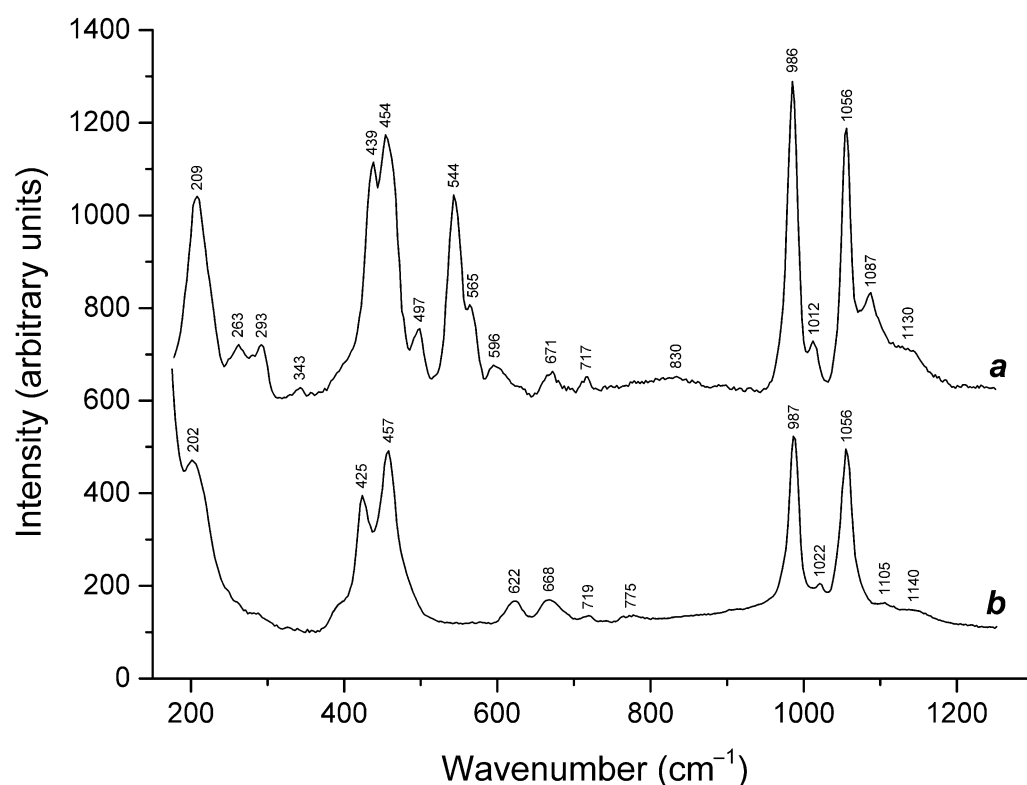


**Figure 6.** Corrected Raman spectra of (a) balliranoite from Tultuyskoe (Sample 1) and (b) holotype balliranoite (Sample 2).

**Table 2.** Raman bands of the studied balliranoite samples and their assignment.

Sample 1	Sample 2	Assignment
Wavenumber (cm <sup>-1</sup> )		
	202	Lattice mode involving libration vibrations of extra-framework components
209s		<i>trans</i> -S <sub>4</sub> bending mode (overlapping with S <sub>5</sub> <sup>2-</sup> bending band) and mixed lattice modes
263		S <sub>3</sub> <sup>•-</sup> bending mode (ν <sub>2</sub> ) and/or S <sub>5</sub> <sup>2-</sup> bending band
293		<i>cis</i> -S <sub>4</sub> <sup>•-</sup> bending or Na–O stretching vibrations
343w		<i>cis</i> -S <sub>4</sub> mixed mode
439s, 454s	425s, 457s	SO <sub>4</sub> <sup>2-</sup> [E(ν <sub>2</sub> ) mode] (overlapping with S <sub>5</sub> <sup>2-</sup> stretching bands for Sample 1)
497		<i>trans</i> -S <sub>4</sub> symmetric stretching mode
544s		S <sub>3</sub> <sup>•-</sup> symmetric stretching (ν <sub>1</sub> ) (possibly, overlapping with the antisymmetric stretching band of <i>gauche</i> - or <i>trans</i> -S <sub>4</sub> )
565		S <sub>5</sub> <sup>•-</sup> stretching or S <sub>3</sub> <sup>•-</sup> antisymmetric stretching (ν <sub>3</sub> ) mode
596		S <sub>2</sub> <sup>•-</sup> stretching mode
671	622, 668	SO <sub>4</sub> bending (ν <sub>4</sub> -F <sub>2</sub> ) mode
717w	719w	CO <sub>3</sub> <sup>2-</sup> in-plane bending vibrations
	775w	Framework mixed band
830 (broad)		S <sub>3</sub> <sup>•-</sup> combination mode (ν <sub>1</sub> + ν <sub>2</sub> ) overlapping with framework mixed and overtone of S <sub>5</sub> <sup>2-</sup> stretching bands
986s	987s	SO <sub>4</sub> <sup>2-</sup> symmetric stretching (ν <sub>1</sub> -A <sub>1</sub> ) mode
1012	1022	Framework and/or SO <sub>3</sub> <sup>2-</sup> stretching vibrations



Table 2. Cont.

Sample 1	Sample 2	Assignment
Wavenumber (cm <sup>-1</sup> )		
1056s	1056s	CO <sub>3</sub> <sup>2-</sup> symmetric stretching vibrations
1087		CO <sub>3</sub> <sup>2-</sup> symmetric stretching vibrations [possibly, overlapping with SO <sub>4</sub> <sup>•-</sup> stretching band ( $\nu_3-F_2$ )]
1130sh	1105w, 1140w	SO <sub>4</sub> <sup>2-</sup> asymmetric ( $\nu_3-F_2$ ) mode [possibly, overlapping with S <sub>2</sub> <sup>•-</sup> overtone ( $2 \times \nu_1$ )]
1640w		S <sub>3</sub> <sup>•-</sup> overtone ( $3 \times \nu_1$ )
2564w		HS <sup>-</sup> stretching mode

Note: w—weak band, s—strong band, sh—shoulder.

After irradiation of Sample 1 with X-rays, its color changed to blue, bands of S<sub>2</sub><sup>•-</sup>, S<sub>4</sub><sup>•</sup>, S<sub>4</sub>, and S<sub>5</sub><sup>2-</sup> in the Raman spectrum disappeared, intensities of the bands corresponding to S<sub>3</sub><sup>•-</sup> increased significantly, and the bands of SO<sub>4</sub><sup>2-</sup>, CO<sub>3</sub><sup>2-</sup>, and HS<sup>-</sup> remained unchanged (curve a in Figure 7, Table 3). The wavenumber of the band of S<sub>3</sub><sup>•-</sup> symmetric stretching vibrations (542 cm<sup>-1</sup>) of the irradiated sample is somewhat less than typical values of analogous bands in sodalite-group minerals (544–546 cm<sup>-1</sup>).

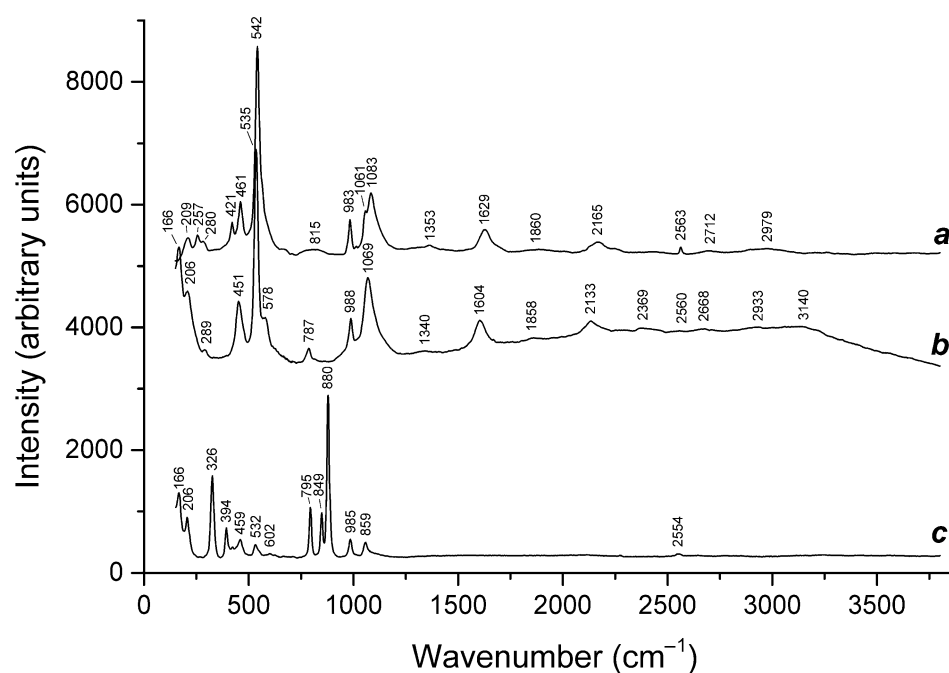


Figure 7. Raman spectra of (a) Sample 1 irradiated with X-rays, (b) Phase 1 in Sample 1 heated in air at 600 °C for 1 h, and (c) Sample 1 heated in air at 800 °C for 6 h.

Table 3. Assignment of Raman bands of the products of irradiation of Sample 1 with X-rays and its heating at 600 °C for 1 h (Phase 1).

Irradiated (Sample 1)	Heated (Phase 1)	Assignment
Wavenumber (cm <sup>-1</sup> )		
209	166s, 206	Low-frequency lattice modes
257	262	S <sub>3</sub> <sup>•-</sup> bending mode ( $\nu_2$ ) and/or S <sub>5</sub> <sup>2-</sup> stretching mode
280w	289w	Lattice modes involving Na <sup>+</sup> cations

Table 3. Cont.

Irradiated (Sample 1)	Heated (Phase 1)	Assignment
Wavenumber (cm <sup>-1</sup> )		
421		S <sub>5</sub> <sup>2-</sup> stretching mode 1 or framework bending vibrations
461	451	SO <sub>4</sub> <sup>2-</sup> [ <i>E</i> (ν <sub>2</sub> ) mode] overlapping with S <sub>5</sub> <sup>2-</sup> stretching bands
542s	535s	S <sub>3</sub> <sup>•-</sup> symmetric stretching (ν <sub>1</sub> ) and/or AlF <sub>6</sub> stretching mode
	578	S <sub>3</sub> <sup>•-</sup> antisymmetric stretching (ν <sub>3</sub> ), possibly, overlapping with the stretching band of S <sub>2</sub> <sup>•-</sup>
815w	787	S <sub>3</sub> <sup>•-</sup> combination mode (ν <sub>1</sub> + ν <sub>2</sub> )
983	988	SO <sub>4</sub> <sup>2-</sup> symmetric stretching vibrations [ <i>A</i> <sub>1</sub> (ν <sub>1</sub> ) mode]
1061, 1083s	1069s	CO <sub>3</sub> <sup>2-</sup> symmetric stretching vibrations
1363w	1340w	S <sub>3</sub> <sup>•-</sup> combination mode (2ν <sub>1</sub> + ν <sub>2</sub> )
1629	1604	S <sub>3</sub> <sup>•-</sup> overtone (3 × ν <sub>1</sub> )
1860w	1858w	S <sub>3</sub> <sup>•-</sup> combination mode (3 × ν <sub>2</sub> + ν <sub>1</sub> )
2165	2133	S <sub>3</sub> <sup>•-</sup> overtone (4 × ν <sub>1</sub> )
	2369w	S <sub>3</sub> <sup>•-</sup> combination mode (4 × ν <sub>2</sub> + ν <sub>1</sub> )
2563w	2560w	HS <sup>-</sup> stretching mode
2712w	2668w	S <sub>3</sub> <sup>•-</sup> overtone (5 × ν <sub>1</sub> )
2979	2933w	S <sub>3</sub> <sup>•-</sup> combination mode (5 × ν <sub>1</sub> + ν <sub>2</sub> )
	3140w	S <sub>3</sub> <sup>•-</sup> overtone (6 × ν <sub>1</sub> )

Heating of Sample 1 in air at 600 °C for 1 h results in the formation of two phases. The Raman spectrum of Phase 1 (curve **b** in Figure 7, Table 3) is similar to that of irradiated Sample 1. The main distinctions of the Raman spectrum of Phase 1 are a lowering of the intensity of the band of HS<sup>-</sup> and significant shifts of all bands of S<sub>3</sub><sup>•-</sup> towards lower wavenumbers.

The Raman spectrum of Phase 2 in Sample 1 in air at 600 °C for 1 h (Figure 8) contains bands of stretching vibrations of HS<sup>-</sup> (at 2566 cm<sup>-1</sup>), CO<sub>3</sub><sup>2-</sup> (at 1058 and 1082 cm<sup>-1</sup>), SO<sub>4</sub><sup>2-</sup> (at 987 cm<sup>-1</sup>), S<sub>2</sub><sup>•-</sup> (at 602 cm<sup>-1</sup>), S<sub>3</sub><sup>•-</sup> (at 535 cm<sup>-1</sup>), and S<sub>5</sub><sup>2-</sup> (at 422 and 457 cm<sup>-1</sup>). The bands of S<sub>5</sub><sup>2-</sup> are narrow and not split, which indicates the presence of only one conformer of this anion, unlike initial Sample 1. Strong luminescence observed in the range of 800–3500 cm<sup>-1</sup> is related to the presence of the S<sub>2</sub><sup>•-</sup> radical anions. Periodic structure of the luminescence spectrum may be a result of interference of laser radiation on thin platelets along cleavage planes formed as a result of cracking the sample during its heating. All other Raman bands of Phase 2 are due to vibrations of the aluminosilicate framework and lattice vibrations (soft acoustic modes). Taking into account that S<sub>3</sub><sup>•-</sup> is the most stable polysulfide species [32], one can suppose that Phase 2 is an intermediate product of the transformation of Sample 1 into Phase 1.

Heating of Sample 1 in air at 800 °C for 6 h resulted in the decomposition of a major part of the aluminosilicate framework and the formation of an orthosilicate whose strong bands are observed at 880, 849, 795, 394, 326, and 166 cm<sup>-1</sup> (curve **c** in Figure 7). The remaining bands correspond to relicts of a cancrinite-type phase with extra-framework S<sub>3</sub><sup>•-</sup>, SO<sub>4</sub><sup>2-</sup>, CO<sub>3</sub><sup>2-</sup>, and HS<sup>-</sup> anions (the bands at 532, 985, 1059, and 2554 cm<sup>-1</sup>, respectively).

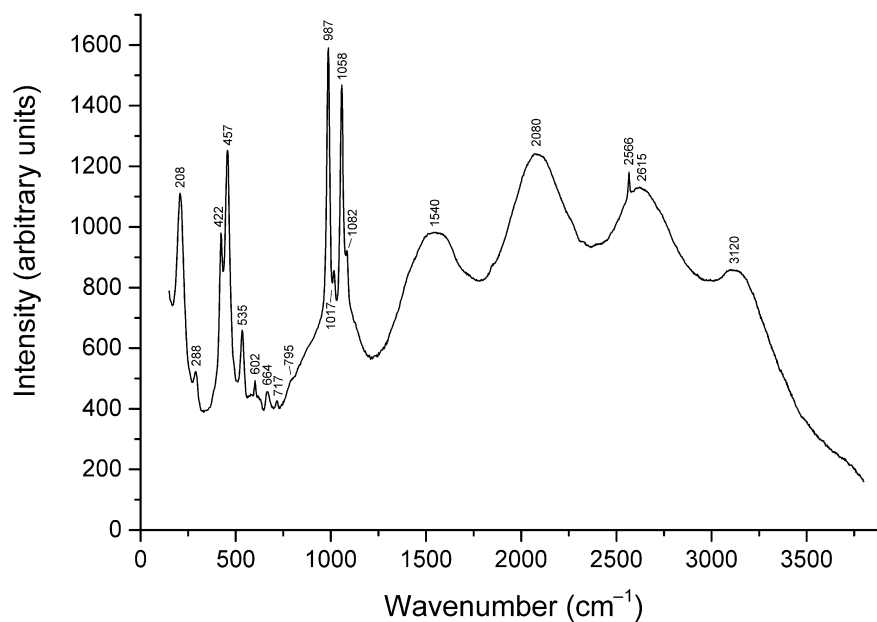


**Figure 8.** Raman spectrum of Phase 2 in Sample 1 heated in air at 600 °C for 1 h.

3.4. Absorption Spectroscopy in the NIR/Vis/UV Ranges

The absorption spectrum of Sample 1 (curve 1 in Figure 9) shows a broad absorption band in the region of 1.45–2.4 eV. With the transition to the ultraviolet region of the spectrum, an increase in absorption is observed. The observed broad band has an asymmetric shape and can be decomposed into two Gaussians with maxima at 2.05 and 2.31 eV and a width of 0.33 eV. Previously, similar bands were observed for S<sub>4</sub>-containing h aüyne and assigned to neutral S<sub>4</sub> molecules having *trans* and *cis* conformations [13].

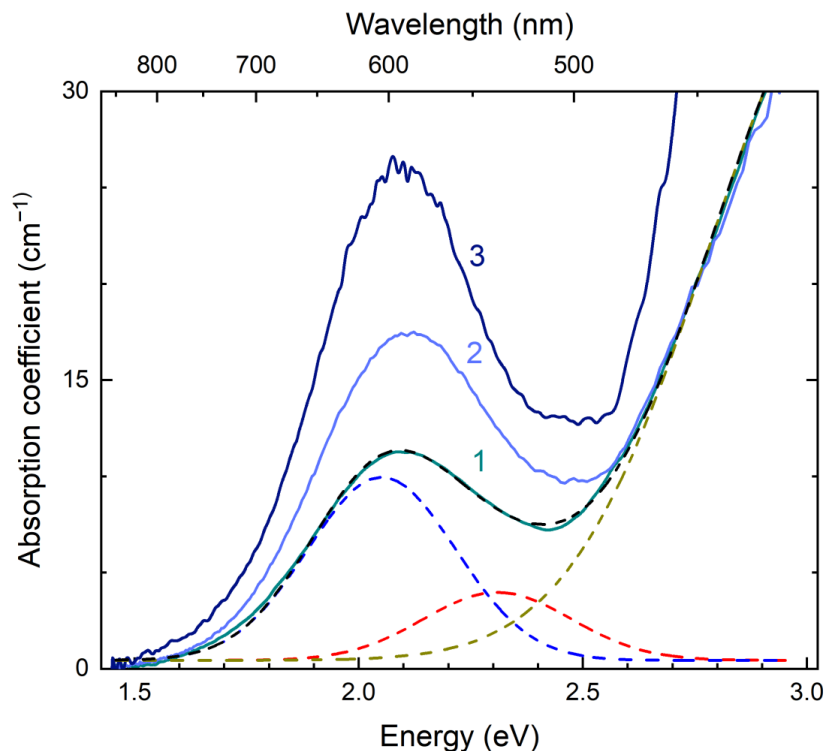


**Figure 9.** Absorption spectra of Sample 1 before irradiation (curve 1), after irradiation with a low-pressure mercury lamp (curve 2), and after irradiation with X-rays (curve 3). Dashed lines show Gaussian components of the absorption spectrum of Sample 1 before irradiation.

After irradiation of Sample 1 with a low-pressure mercury lamp (with wavelengths of 193 and 253 nm) or X-ray irradiation, the absorption in the region of 1.6–2.4 eV (with a maximum at about 2.1 nm) increases (Figure 9, curves 2 and 3) and the sample acquires a deep blue color.

### 3.5. ESR Spectroscopy

In the ESR spectrum of the original Sample 1, only a sextet from  $\text{Mn}^{2+}$  (with a fine structure of the sextet components) was observed. After irradiation, an additional ESR signal appears, with the  $g$ -tensor components  $g_1 = 2.053$ ,  $g_2 = 2.040$  and  $g_3 = 2.001$  (Figure 10). The intensity of the  $\text{Mn}^{2+}$  sextet does not change after irradiation.

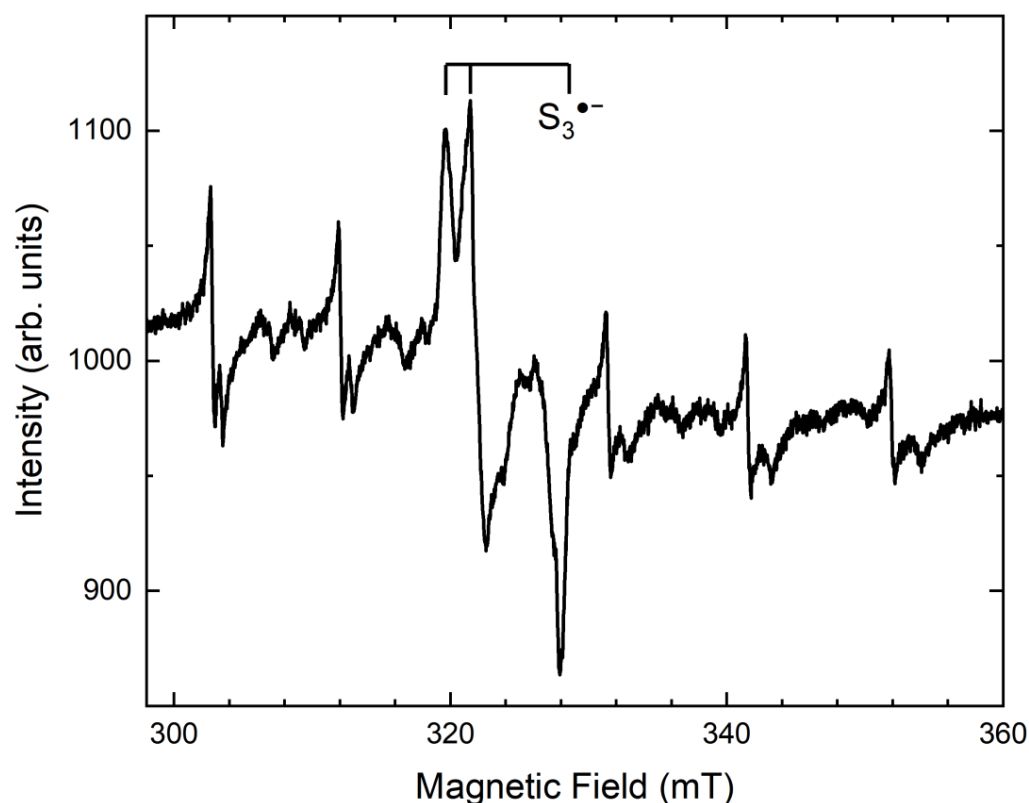


**Figure 10.** ESR spectrum of irradiated balliranoite (Sample 1). The vertical lines show the signal from  $\text{S}_3^{\bullet-}$  radical anions.

### 3.6. Luminescence Spectroscopy

When Sample 1 is excited with a 405 nm radiation, a broad luminescence band is observed with a maximum at 645 nm and a pronounced vibrational structure (Figure 11). The distance between phonon repetitions is about  $595 \text{ cm}^{-1}$ . Similar luminescence bands were previously observed for other microporous minerals in the form of a wide band with a maximum at 580 nm for marinellite, 620 nm for biachellalite, 640 nm for tugtupite [14], 610 nm for hackmanite [37], 625 nm for sapozhnikovite [7], 650 nm for haüyne [5,13], 600 nm for afghanite, 640 nm for nosean, and 630 nm for kyanoxalite [12].

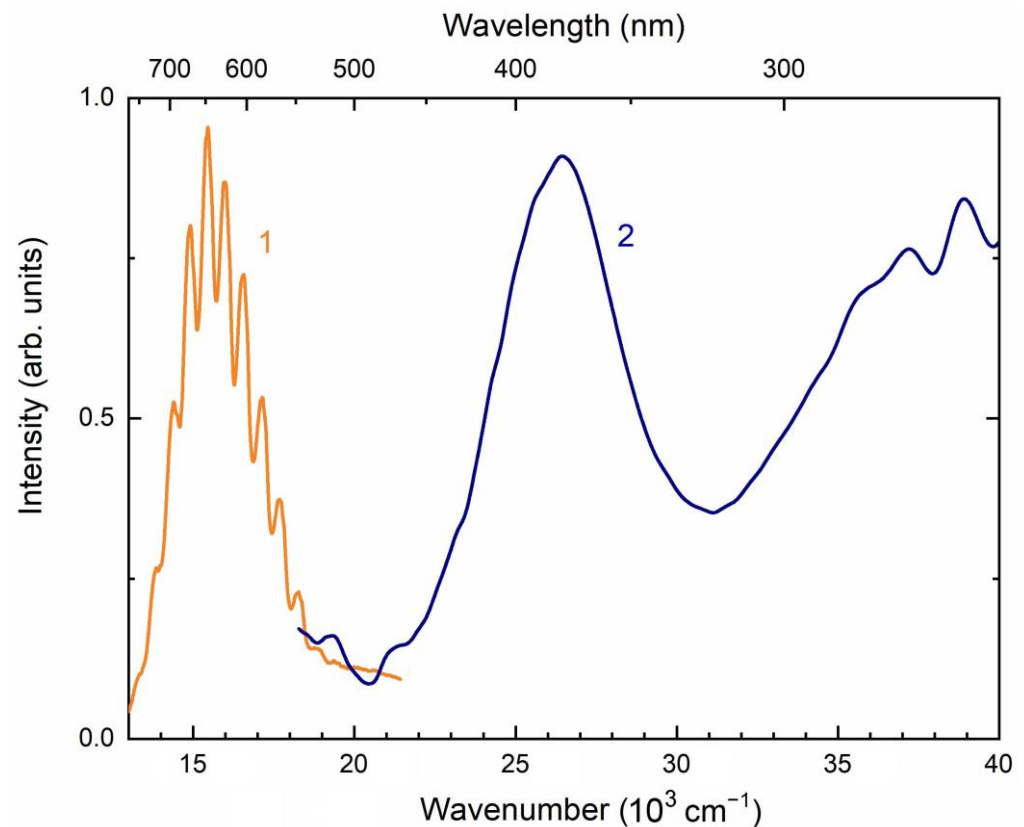


**Figure 11.** Luminescence spectrum of Sample 1 excited with a 405 nm radiation (curve 1) and luminescence excitation spectrum of Sample 1 monitored at 650 nm (curve 2), both measured at 77 K.

### 3.7. Crystal Structure

The crystal structure was solved with direct methods and refined to  $R = 0.0476$  for 1191 independent reflections with  $I > 2\sigma(I)$  using SHELX software package [38] with anisotropic treatment of all atoms except S, C, and corresponding O atoms of sulfate and carbonate groups. The structure was studied in the frame of hexagonal space group  $P6_3$ . The unit cell parameters are  $a = 12.6874(4)$ ,  $c = 5.32039(17)$  Å,  $V = 741.68(5)$  Å<sup>3</sup>. As previously reported holotype balliranoite from the Somma–Vesuvio volcanic complex [19], the studied crystal is merohedrally twinned with an inversion center as a twinning operator; the 0.54:0.46 ratio of twin components was found.

In the crystal structure of the studied crystal as well as in the holotype balliranoite [19], Al and Si atoms are ordered among tetrahedral sites, which is typical for cancrinite-group minerals. The average  $\langle\text{Si–O}\rangle$  and  $\langle\text{Al–O}\rangle$  distances in tetrahedra are 1.625 and 1.722 Å, respectively. The aluminosilicate framework is the same as reported for holotype balliranoite.

Calcium cations are located at the centers of bases of the cancrinite cages. The Ca site is characterized by the partial occupancy factor of 0.949(14).  $\text{Ca}^{2+}$  cations occupy eight-fold polyhedra with six Ca–O bonds varying from 2.566(5) to 2.629(5) Å and two Ca–Cl bonds with the distances of 2.646(8) and 2.686(8) Å. Unlike the structure of balliranoite from the Somma–Vesuvio volcanic complex, in the studied crystal all  $\text{Cl}^-$  anions are statistically distributed over three symmetry-related sites slightly offset from the three-fold axis, and at the last stages of the refinement their site occupancy factors were fixed at 0.33.

Two Na-dominant sites statistically replacing each other are located in the wide channel of the framework. The occupancy factors of these sites refined on the basis of the Na scattering curve are 0.51(8) and 0.56(9). This corresponds to the total number of electrons of 11.77 which is in a good agreement with chemical data and corresponds to the (Ca,K) admixture of 10%.

Three crystallographically nonequivalent C sites were found from difference Fourier synthesis at the center of the wide channel. Two of them (C1 and C2) are located very close to the corresponding sites in the structure of holotype balliranoite [19], while the third site (C3) is a new one. A set of constraints was introduced in the refinement. In particular,  $\text{CO}_3^{2-}$  groups were considered to be planar, with the same  $z$  coordinate of C and O atoms. The position of the S site found in balliranoite from the Somma–Vesuvio volcanic complex [19] is vacant in the studied sample. The refinement showed that two of three C sites (C2 and C3) contain additional components, and it was assumed that S atoms statistically replace C at their sites. O atoms of the  $\text{C1O}_3$  groups showed higher occupancy factor than C1 and were assumed to participate also in  $\text{SO}_4$  tetrahedra forming the common base of two tetrahedra with opposite orientation. The fourth vertices of the  $\text{SO}_4$  tetrahedra were fixed at corresponding distances from the S sites. At the last stage of the refinement, the occupancies of C, S, and corresponding O sites were fixed according to chemical data and for preservation of reliable parameters of atomic displacements: C1, C2, C3 sites have site occupancy factors of 0.18, 0.08, and 0.09, respectively, and S atoms replacing C2 and C3—0.06 and 0.03, respectively. S atoms of polysulfide groups could not be localized because of their low occupancy factors and strong disordering in the wide channel. The arrangement of the main extra-framework components in the wide channel is shown in Figure 12.

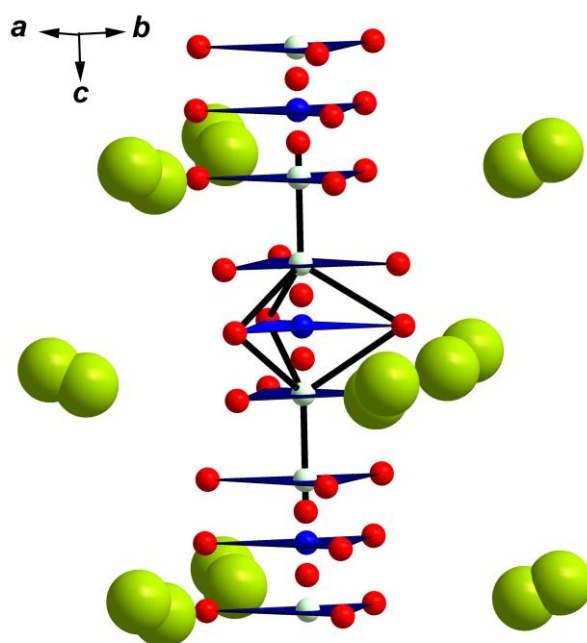


**Figure 12.** Filling of the wide channel in the structure of sulfide-bearing balliranoite (Sample 1). Na-dominant sites are shown as big green balls, C1 site is blue, and (C,S) sites are small light-green balls. Possible S–O and C–O bonds are shown.

## 4. Discussion

### 4.1. Crystal-Chemical Features of Sulfide-Bearing Balliranoite

Balliranoite from Tultuyskoe is a bright example illustrating complex chemistry and crystal chemistry of sulfur in minerals with microporous structures. The crystal-chemical formula of Sample 1 derived based on chemical data and crystal structure refinement is  $\text{H}_x(\text{Na}_{5.3}\text{Ca}_{0.6}\text{K}_{0.1})\text{Ca}_2(\text{Si}_6\text{Al}_6\text{O}_{24})\text{Cl}_2[(\text{CO}_3)_{0.7}(\text{SO}_4)_{0.2}\text{S}^*_{0.95}\text{Cl}_{0.1}]\cdot n\text{H}_2\text{O}$ , where formula coefficients are rounded, non-cationic species occurring in the wide channel are given in square brackets,  $\text{S}^*_{0.95}$  is total sulfide sulfur (in the  $\text{S}_2^{\bullet-}$ ,  $\text{S}_3^{\bullet-}$ ,  $\text{S}_4$ ,  $\text{S}_5^{2-}$ , and  $\text{HS}^-$  groups), and  $\text{H}_x$  is hydrogen belonging to  $\text{HS}^-$  groups,  $x \sim 0.1$  and  $n \sim 0.1$ . Based on the charge-balance requirement, the total charge of  $\text{S}^*_{0.95}$  is about  $-0.8$ , which indicates a significant portion of  $\text{S}^{2-}$  (as a part of  $\text{HS}^-$  or isolated  $\text{S}^{2-}$  anions) or the presence

of additional disordered  $\text{SO}_4^{2-}$  groups which could not be localized during the crystal structure refinement.

The general structural formula of sulfide-bearing balliranoite can be written as  $(\text{Na,Ca,K})_6\text{Ca}_2(\text{Si}_6\text{Al}_6\text{O}_{24})(\text{Cl}^-, \text{HS}^-)_2(\text{CO}_3^{2-}, \text{SO}_4^{2-}, \text{S}_2^{\bullet-}, \text{S}_3^{\bullet-}, \text{S}_4, \text{S}_5^{2-}, \text{Cl}^-, \text{HS}^-)_{1+y} \cdot n\text{H}_2\text{O}$ , where  $y < 1$ ,  $n \ll 1$ , and each of the  $\text{S}_4$  and  $\text{S}_5^{2-}$  species is present in two conformation states.

Specific features of the studied sample are an unusual diversity and strong disordering of extra-framework components. In particular, in the structure of sulfide-bearing balliranoite (Sample 1) there are three sites of carbonate groups instead of two sites in the holotype balliranoite sample. This is in agreement with the IR spectrum showing additional bands of asymmetric C–O stretching vibrations (at 1395, 1434, and 1477  $\text{cm}^{-1}$ ) and non-degenerate bands of  $\text{CO}_3^{2-}$  out-of-plane bending vibrations (at 880  $\text{cm}^{-1}$ ) as compared to the holotype sample.

Among S atoms, only those belonging to  $\text{SO}_4^{2-}$  groups with low occupancies were localized during the crystal structure refinement. We assume that S sites of polysulfide anions, radical anions, and molecules are characterized by very low site occupancy factors and are strongly disordered in the wide channel. This does not allow their localization using XRD data. All attempts to lower symmetry for a better localization of sulfide sulfur were unsuccessful.

#### 4.2. Indicatory Significance of Extra-Framework Species in Balliranoite

The composition of extra-framework species in feldspathoids is considered as a marker of important characteristics of mineral-forming media, including fugacities of volatile components ( $\text{H}_2\text{O}$ ,  $\text{O}_2$ ,  $\text{CO}_2$ , HF,  $\text{SO}_2$ , and polysulfide compounds) [5,7,14,39–41].  $\text{HS}^-$  and  $\text{S}_5^{2-}$  anions occurring in feldspathoids are indicators of highly reducing conditions of mineral formation whereas extra-framework  $\text{CO}_2$  molecules, generally typical for members of the cancrinite and sodalite groups [5,7,12–14], are absent in minerals containing  $\text{HS}^-$  and  $\text{S}_5^{2-}$  anions [7,42]. In this reference, it is important to note that all oxygen-bearing minerals associated with sulfide-bearing balliranoite (Sample 1) do not contain iron in amounts exceeding the detection limit of the electron microprobe analysis (practically, all iron occurs in pyrrhotite). In particular, the charge-balanced empirical formula of white iron-free pargasite from this assemblage is  $\text{K}_{0.07}\text{Na}_{1.01}\text{Ca}_{1.92}(\text{Mg}_{4.12}\text{Al}_{0.65}\text{Ti}_{0.13})(\text{Si}_{6.38}\text{Al}_{1.62}\text{O}_{22})(\text{OH})_2$ . On the contrary, pargasite and phlogopite from the association with holotype balliranoite contain significant amounts of iron whereas sulfides are absent there.

In situ Raman spectroscopy was used to identify various S-bearing species in aqueous fluids on a model system prepared from potassium thiosulfate, sulfide, and sulfate, in a wide range of sulfur concentration, acidity, temperature, and pressure [40]. According to these data, in the hydrothermal solutions and supercritical fluid phases, the trisulfur radical anion  $\text{S}_3^{\bullet-}$  is thermodynamically stable, along with sulfate anion, from 200 °C to at least 700 °C. The  $\text{S}_2^{\bullet-}$  radical anion was detected in the range of 450–500 °C. In S-rich solutions, maximum abundance of neutral polysulfide groups  $\text{S}_n$  was observed at around 300 °C. At temperatures below 500 °C, the amount of  $\text{S}_3^{\bullet-}$  is up to 10% of total dissolved sulfur, but at 600–700 °C the fraction of  $\text{S}_3^{\bullet-}$  reaches 50% of total sulfur.

Fluid inclusions in quartz synthesized from S-bearing solutions contain  $\text{SO}_4^{2-}$  and  $\text{HS}^-$  anions, which are stable up to 500 °C and are in equilibrium with the  $\text{S}_3^{\bullet-}$  radical anion whose fraction increases with temperature [43].

According to the calculated phase diagram of the Fe–S system [44], at the molar ratios  $\text{S}/(\text{Fe}+\text{S}) > 0.5$  pyrrhotite cannot coexist with pyrite at temperatures above 700 °C or below 300 °C. On the other hand, in the Fe–O–S system, at ambient pressure pyrrhotite is thermodynamically stable only at temperatures above 500 °C. Under highly reducing conditions, pyrrhotite is stable only at temperatures just slightly exceeding 500 °C [45] which corresponds to the lowest values for lazurite-bearing metasomatites of the Baikal Lake area, which formed at low pressures, in zones of tectonic unloading [46].

Phase diagram of the system Fe–S–O–H constructed at 500 °C and 4.0 kbar shows that under these conditions pyrrhotite is stable only at  $\text{pH} < 9$  and  $\log f_{\text{O}_2} < -20$ , but only in

the interval  $-21 < \log fO_2 < -20$  can pyrrhotite exist in thermodynamical equilibrium with pyrite [47].

Polysulfide groups other than  $S_3^{\bullet-}$  are unstable above 700 °C [13,15]. Moreover, there are indications of transformations of a yellow chromophore (presumably,  $S_2^{\bullet-}$ ) into  $S_3^{\bullet-}$  as a result of long-time heating of a lazurite-related sodalite-group mineral at 500 °C [46]. Thus, one can suppose that balliranoite from Tultuyskoe crystallized under highly reducing, low-temperature (below 500 °C), near-neutral or weak-acidic conditions. It is to be noted that a major part of cancrinite-group minerals and low-symmetry sodalite-group minerals (including vladimirivanovite), which occur in lapis lazuli deposits and are most abundant in the Tultuyskoe deposit, crystallized after cubic lazurite and members of the lazurite–häüyne solid-solution series [21,46,48,49].

Holotype balliranoite (Sample 2) formed in a volcanic complex does not contain sulfide sulfur. Luminescence observed in the Raman spectrum indicates that this sample contains a trace amount of  $Fe^{3+}$ , unlike Sample 1 which is iron-free. IR spectrum of Sample 2 shows the presence of extra-framework  $CO_2$  molecules. All these signs indicate that Sample 2 crystallized at relatively more oxidizing conditions as compared to Sample 1 and Sample 3.

#### 4.3. Radiation-Induced Transformations of Sulfide-Bearing Balliranoite

Previously, the appearance of a blue color and ESR signal as a result of irradiation was observed for a number of other carbonate minerals, including layered silicates of the carletonite group [50,51], cancrinite [52,53], and kyanoxalite [12]. After irradiation of these minerals, a band with a maximum in the range of 1.8–2.0 eV appeared in the absorption spectra, and an ESR signal with  $g_1 = 2.018$ ,  $g_2 = 2.014$ , and  $g_3 = 2.008$  was observed. These bands are associated with the  $CO_3^{\bullet-}$  radical anion. However, in the case of balliranoite (Sample 1), both the ESR signal and the absorption spectrum differ significantly from those for the  $CO_3^{\bullet-}$  radical anion.

The observed absorption peaking at about 2.1 eV and the observed ESR spectrum of the irradiated Sample 1 can be associated with the presence of  $S_3^{\bullet-}$  radical anions. In many microporous minerals including lazurite [6], häüyne [15], kyanoxalite and afghanite [12], and marinellite [14], a similar ESR signal and an absorption band in the 2.0–2.1 eV region associated with  $S_3^{\bullet-}$  radical anions were previously observed (Table 4). The ESR spectra of the  $S_3^{\bullet-}$  radical anion in kyanoxalite and afghanite are most close to the ESR spectrum of the irradiated Sample 1 (Table 3).

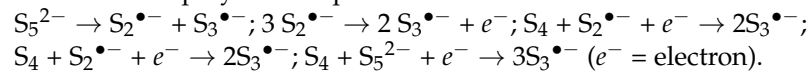
**Table 4.** Bands of  $S_3^{\bullet-}$  in ESR and optical absorption spectra of feldspathoids.

Mineral	g-Factor Components	Absorption Maximum (eV)
Kyanoxalite	2.050, 2.038, 2.002 [12]	2.09 [12]
Afgranite	2.057–2.060, 2.038, 2.002 [12]	2.09 [12]
Häüyne	2.056, 2.041, 2.008 [15]	2.05 [15]
Häüyne	2.046, 2.031, 2.010 [5]	2.06 [5]
Nosean	2.041, 2.031, 2.004 [12]	2.07 [14]
Lazurite	2.030, 2.030, 2.030 [6]	2.07 [5]
Vladimirivanovite	2.034, 2.004 [14]	2.00 [14]
Marinellite	2.039, 2.008 [14]	2.10 [14]
Biachellaite	2.058, 2.036, 2.002 [14]	No data
Balliranoite	2.053, 2.040, 2.001 (this work)	2.1 [14]

This ESR signal was not detected in the original balliranoite sample, whereas after irradiation it appears and the color of the sample becomes blue. Since this effect is also observed under far ultraviolet irradiation, one can suppose that photolysis of  $S_4$  molecules with the formation of  $S_3^{\bullet-}$  may take place. Previously, photolysis of  $S_4$  molecules with the formation of  $S_2^{\bullet-}$  was observed upon irradiation with an excimer laser at a wavelength of 248 nm [54]. Given the initial composition of Sample 1, data on the ESR and Raman spectra of irradiated Sample 1, and the fact that the radical anion  $S_3^{\bullet-}$  is one of the most



stable forms of sulfide sulfur [14], the general scheme of the observed radiation-induced transformations of polysulfide species can be written as follows:



Observed luminescence (Figure 11) is associated with  $S_2^{\bullet-}$  radical anions, similarly to other microporous minerals [5,7,12–14,37]. The excitation bands at 255–375 nm could be attributed to the transitions to  $\pi$  and  $\pi^*$  excited states of  $S_2^{\bullet-}$  radical anions. However, higher energy excitation bands at 255 and 265 nm may also correspond to the excitation of the balliranoite framework [53].

#### 4.4. Thermal Transformations of Sulfide-Bearing Balliranoite

Changes in the Raman spectrum of sulfide-bearing balliranoite when it is heated are similar to those observed when it is irradiated with X-rays. At high temperatures, the  $S_3^{\bullet-}$  radical anion is the most stable species containing sulfide sulfur. Moreover, a part of sulfate anions transforms into  $S_3^{\bullet-}$  on heating.

As it was shown above, heating of Sample 1 in air at 800 °C for 6 h results in the formation of an orthosilicate. This result is unexpected, taking into account that other carbonate cancrinite-group minerals (cancrinite and cancrisilite) transform into a nepheline-type aluminosilicate on heating above 700 °C [55]. On the other hand, the nepheline-related compound carnegieite,  $\text{Na}(\text{AlSiO}_4)$ , has a polymorph, the orthosilicate  $\text{NaAl}(\text{SiO}_4)$ , which is stable above 690 °C (URL [https://materials.springer.com/isp/crystallographic/docs/sd\\_1502237](https://materials.springer.com/isp/crystallographic/docs/sd_1502237) accessed on 24 May 2023). Thus, the hypothetical scheme of transformations of Sample 1 on heating up to 800 °C is:  $\text{Na}_{5.4}\text{K}_{0.1}\text{Ca}_{2.4}(\text{Si}_6\text{Al}_6\text{O}_{24})\text{Cl}_2[(\text{CO}_3)_{0.7}(\text{SO}_4)_{0.18}\text{S}^{*0.95}\text{Cl}_{0.1}(\text{H}_2\text{O})_{0.16}] \rightarrow (\text{Na,K,Ca})(\text{AlSiO}_4) + \text{Ca-oxides/chlorides} + \text{CO}_2(\text{gas}) + \text{SO}_2(\text{gas}) + \text{H}_2\text{O}(\text{gas}); (\text{Na,K,Ca})(\text{AlSiO}_4) \rightarrow (\text{Na,K,Ca})\text{Al}(\text{SiO}_4)$ , where  $(\text{Na,K,Ca})(\text{AlSiO}_4)$  is nepheline.

A low-frequency shift of the band of  $S_3^{\bullet-}$  symmetric stretching vibrations after irradiation (towards  $542 \text{ cm}^{-1}$ ) and especially as a result of heating (towards  $535 \text{ cm}^{-1}$  at  $600^\circ$  and  $532 \text{ cm}^{-1}$  at  $800^\circ$ ) indicates that transformations of different S-bearing groups into  $S_3^{\bullet-}$  radical anion result in removal of the steric load on the latter.

## 5. Conclusions

The crystal-chemical data of sulfide-bearing balliranoite from Tultuyskoe (Sample 1) obtained in this work illustrate a very complex chemical behavior of sulfur-bearing and other extra-framework components in feldspathoids belonging to the cancrinite and sodalite groups. The general crystal-chemical formula of Sample 1 is  $(\text{Na,K,Ca})_6\text{Ca}_2(\text{Si}_6\text{Al}_6\text{O}_{24})(\text{Cl}^-, \text{HS}^-)_2(\text{CO}_3^{2-}, \text{SO}_4^{2-}, \text{S}_2^{\bullet-}, \text{S}_3^{\bullet-}, \text{S}_4, \text{S}_5^{2-}, \text{Cl}^-, \text{HS}^-) \cdot n\text{H}_2\text{O}$ .

The  $\text{HS}^-$  and  $\text{S}_5^{2-}$  anions occurring in this sample were earlier detected only in three feldspathoids (bystrite, sulfhydrylbystrite, and sapozhnikovite) which crystallized under reducing conditions. The absence of  $\text{CO}_2$  molecules among extra-framework species and the absence of iron in associated oxygen-bearing minerals (all iron occurs in pyrrhotite) confirm reducing conditions of the formation of sulfide-bearing balliranoite.

The absorption spectrum of balliranoite from Tultuyskoe in the visible range is a superposition of partial spectra of polysulfide groups which are yellow ( $\text{S}_2^{\bullet-}$  and  $\text{S}_5^{2-}$ ), blue ( $\text{S}_3^{\bullet-}$ ), pink (*cis*- $\text{S}_4$ ), and green (*trans*- $\text{S}_4$ ) chromophores. Luminescence of this sample is mainly due to  $\text{S}_2^{\bullet-}$  centers.

Radiation-induced transformations of polysulfide species ( $\text{S}_2^{\bullet-}$ ,  $\text{S}_4^{\bullet-}$ , *cis*- and *trans*- $\text{S}_4$ , and  $\text{S}_5^{2-}$ ) in the studied mineral result in the formation of  $\text{S}_3^{\bullet-}$  which is the most stable polysulfide group. However, no radiolysis of  $\text{CO}_3^{2-}$ ,  $\text{SO}_4^{2-}$ , and  $\text{HS}^-$  anions was observed.

Thermal transformations of sulfide-bearing balliranoite at  $600^\circ$  result in the transformation of most initial sulfide-bearing groups into  $\text{S}_3^{\bullet-}$  via intermediate  $\text{S}_2^{\bullet-}$ . At  $800^\circ\text{C}$ , decomposition of the aluminosilicate framework and formation of an orthosilicate is observed.

**Author Contributions:** Conceptualization, N.V.C., A.N.S., R.Y.S. and I.V.P.; methodology, N.V.C., R.Y.S. and M.F.V.; collecting of minerals, A.N.S., N.V.C. and I.V.P.; investigation, R.Y.S., N.V.C., M.F.V., N.V.Z., N.V.P. and D.A.K.; original manuscript draft preparation, N.V.C., R.Y.S. and N.V.Z.; manuscript review and editing, N.V.C., R.Y.S., N.V.Z. and I.V.P.; figures, N.V.C., R.Y.S. and N.V.Z. All authors have read and agreed to the published version of the manuscript.

**Funding:** Raman: ESR and UV-Vis-near IR spectroscopy, spectroscopy of luminescence, single-crystal X-ray structure study, crystal-chemical analysis and data interpretation and summarizing were supported by the Russian Science Foundation, grant No. 22-17-00006 (for N.V.C., R.Yu.S., N.V.Z., M.F.V., N.V.P. and I.V.P.), <https://rscf.ru/project/22-17-00006/> (accessed on 24 May 2023). Identification of minerals, chemical analyses, as well as middle-range IR spectroscopy investigation were carried out in accordance with the state task, state registration No. AAA-A19-119092390076-7 (for N.V.C.).

**Data Availability Statement:** Not applicable.

**Acknowledgments:** The authors are grateful to Mikhail V. Voronin for a fruitful discussion.

**Conflicts of Interest:** The authors declare no conflict of interest.

## References

1. Ballirano, P.; Maras, A.; Buseck, P.R. Crystal chemistry and IR spectroscopy of Cl- and SO<sub>4</sub>-bearing cancrinite-like minerals. *Am. Mineral.* **1996**, *81*, 1003–1012. [[CrossRef](#)]
2. Bonaccorsi, E.; Merlino, S. Modular microporous minerals: Cancrinite-davyne group and C-S-H phases. *Rev. Mineral. Geochem.* **2005**, *57*, 241–290. [[CrossRef](#)]
3. Merlino, S. Feldspathoids: Their average and real structures. In *Feldspars Feldspathoids*; NATO ASI Series; Brown, W.L., Ed.; Springer: Dordrecht, The Netherlands, 1984; Volume 137, pp. 435–470. [[CrossRef](#)]
4. Chukanov, N.V.; Aksenov, S.M.; Rastsvetaeva, R.K. Structural chemistry, IR spectroscopy, properties, and genesis of natural and synthetic microporous cancrinite- and sodalite-related materials: A review. *Micropor. Mesopor. Mater.* **2021**, *323*, 111098. [[CrossRef](#)]
5. Chukanov, N.V.; Sapozhnikov, A.N.; Shendrik, R.Y.; Vigasina, M.F.; Steudel, R. Spectroscopic and crystal-chemical features of sodalite-group minerals from gem lazurite deposits. *Minerals* **2020**, *10*, 1042. [[CrossRef](#)]
6. Sapozhnikov, A.N.; Tauson, V.L.; Lipko, S.V.; Shendrik, R.Y.; Levitskii, V.I.; Suvorova, L.F.; Chukanov, N.V.; Vigasina, M.F. On the crystal chemistry of sulfur-rich lazurite, ideally Na<sub>7</sub>Ca(Al<sub>6</sub>Si<sub>6</sub>O<sub>24</sub>)(SO<sub>4</sub>)(S<sub>3</sub>)<sup>-n</sup>H<sub>2</sub>O. *Am. Mineral.* **2021**, *106*, 226–234. [[CrossRef](#)]
7. Chukanov, N.V.; Zubkova, N.V.; Pekov, I.V.; Shendrik, R.Y.; Varlamov, D.A.; Vigasina, M.F.; Belakovskiy, D.I.; Britvin, S.N.; Yapaskurt, V.O.; Pushcharovsky, D.Y. Sapozhnikovite, Na<sub>8</sub>(Al<sub>6</sub>Si<sub>6</sub>O<sub>24</sub>)(HS)<sub>2</sub>, a new sodalite-group mineral from the Lovozero alkaline massif, Kola Peninsula. *Mineral. Mag.* **2022**, *86*, 49–59. [[CrossRef](#)]
8. Chukanov, N.V.; Vigasina, M.F.; Zubkova, N.V.; Pekov, I.V.; Schäfer, C.; Kasatkin, A.V.; Yapaskurt, V.O.; Pushcharovsky, D.Y. Extra-framework content in sodalite-group minerals: Complexity and new aspects of its study using infrared and Raman spectroscopy. *Minerals* **2020**, *10*, 363. [[CrossRef](#)]
9. Chukanov, N.V.; Zubkova, N.V.; Varlamov, D.A.; Pekov, I.V.; Belakovskiy, D.I.; Britvin, S.N.; Van, K.V.; Ermolaeva, V.N.; Vozchikova, S.A.; Pushcharovsky, D.Y. Steudelite, (Na<sub>3</sub>□)[(K,Na)<sub>17</sub>Ca<sub>7</sub>]Ca<sub>4</sub>(Al<sub>24</sub>Si<sub>24</sub>O<sub>96</sub>)(SO<sub>3</sub>)<sub>6</sub>F<sub>6</sub>·4H<sub>2</sub>O, a new cancrinite-group mineral with afghanite-type framework topology. *Phys. Chem. Miner.* **2022**, *49*. [[CrossRef](#)]
10. Chukanov, N.V.; Pekov, I.V.; Olysysh, L.V.; Massa, W.; Zadov, A.E.; Rastsvetaeva, R.K.; Vigasina, M.F. Kyanoxalite, a new cancrinite-group mineral species with extraframework oxalate anion from the Lovozero alkaline pluton, Kola peninsula. *Geol. Ore Depos.* **2010**, *52*, 778–790. [[CrossRef](#)]
11. Chukanov, N.V.; Pekov, I.V.; Olysysh, L.V.; Zubkova, N.V.; Vigasina, M.F. Crystal chemistry of cancrinite-group minerals with AB-type frameworks. II. IR spectroscopy and its crystal chemical implications: Review and new data. *Can. Mineral.* **2011**, *49*, 1151–1164. [[CrossRef](#)]
12. Chukanov, N.V.; Vigasina, M.F.; Shendrik, R.Y.; Varlamov, D.A.; Pekov, I.V.; Zubkova, N.V. Nature and isomorphism of extra-framework components in cancrinite- and sodalite-related minerals: New data. *Minerals* **2022**, *12*, 729. [[CrossRef](#)]
13. Chukanov, N.V.; Zubkova, N.V.; Pekov, I.V.; Giester, G.; Pushcharovsky, D.Y. Sulfite analogue of alloriite from Sacrofano, Latium, Italy: Crystal chemistry and specific features of genesis. *Geol. Ore Depos.* **2021**, *63*, 793–804. [[CrossRef](#)]
14. Chukanov, N.V.; Shchipalkina, N.V.; Shendrik, R.Y.; Vigasina, M.F.; Tauson, V.L.; Lipko, S.V.; Varlamov, D.A.; Shcherbakov, V.D.; Sapozhnikov, A.N.; Kasatkin, A.V.; et al. Isomorphism and mutual transformations of S-bearing ligands in feldspathoids with microporous structures. *Minerals* **2022**, *12*, 1456. [[CrossRef](#)]
15. Chukanov, N.V.; Shendrik, R.Y.; Vigasina, M.F.; Pekov, I.V.; Sapozhnikov, A.N.; Shcherbakov, V.D.; Varlamov, D.A. Crystal chemistry, isomorphism, and thermal conversions of extra-framework components in sodalite-group minerals. *Minerals* **2022**, *12*, 887. [[CrossRef](#)]
16. Lo Giudice, A.; Angelici, D.; Re, A.; Gariani, G.; Borghi, A.; Calusi, S.; Giuntini, L.; Massi, M.; Castelli, L.; Taccetti, F.; et al. Protocol for lapis lazuli provenance determination: Evidence for an Afghan origin of the stones used for ancient carved artefacts kept at the Egyptian Museum of Florence (Italy). *Archaeol. Anthropol. Sci.* **2017**, *9*, 637–651. [[CrossRef](#)]

17. Tauson, V.L.; Sapozhnikov, A.N.; Shinkareva, S.N.; Lustenberg, E.E. Indicative properties of lazurite as a member of clathrasil mineral family. *Dokl. Earth Sci.* **2011**, *441*, 1732–1737. [[CrossRef](#)]
18. Rejmak, P. Computational refinement of the puzzling red tetrasulfur chromophore in ultramarine pigments. *Phys. Chem. Chem. Phys.* **2020**, *22*, 22684–22698. [[CrossRef](#)]
19. Chukanov, N.V.; Zubkova, N.V.; Pekov, I.V.; Olysysh, L.V.; Bonaccorsi, E.; Pushcharovsky, D.Y. Balliranoite,  $(\text{Na,K})_6\text{Ca}_2(\text{Si}_6\text{Al}_6\text{O}_{24})\text{Cl}_2(\text{CO}_3)$ , a new cancrinite-group mineral from Monte Somma—Vesuvio volcanic complex, Italy. *Eur. J. Mineral.* **2010**, *22*, 113–119. [[CrossRef](#)]
20. Ballirano, P.; Bonaccorsi, E.; Merlino, S.; Maras, A. Carbonate groups in davyne: Structural and crystal-chemical considerations. *Can. Mineral.* **1998**, *36*, 1285–1292.
21. Sapozhnikov, A.N.; Chukanov, N.V.; Suvorova, L.F.; Feoktistova, L.P.; Bogdanova, L.A. Davyne from the Tultui lazurite deposit, Baikal Lake area. *Zap. Vserossiiskogo Miner. Obs. (Proc. Russ. Mineral. Soc.)* **2006**, *135*, 77–84. (In Russian)
22. Bonaccorsi, E.; Merlino, S.; Pasero, M. Davyne: Its structural relationships with cancrinite and vishnevite. *Neues Jahrb. Mineral. Monatsch.* **1990**, *3*, 97–112.
23. Della Ventura, G.; Bellatreccia, F.; Parodi, G.C.; Cámara, F.; Piccinini, M. Single-crystal FTIR and X-ray study of vishnevite, ideally  $[\text{Na}_6(\text{SO}_4)]_2[\text{Na}_2(\text{H}_2\text{O})_2][\text{Si}_6\text{Al}_6\text{O}_{24}]$ . *Am. Mineral.* **2007**, *92*, 713–721. [[CrossRef](#)]
24. Pekov, I.V.; Olysysh, L.V.; Chukanov, N.V.; Zubkova, N.V.; Pushcharovsky, D.Y.; Van, K.V.; Giester, G.; Tillmanns, E. Crystal chemistry of cancrinite-group minerals with AB-type frameworks. I. Chemical and structural variations: Review and new data. *Can. Mineral.* **2011**, *49*, 1129–1150. [[CrossRef](#)]
25. Chukanov, N.V.; Zubkova, N.V.; Kazheva, O.N.; Varlamov, D.A.; Pekov, I.V.; Belakovskiy, D.I.; Ternes, B.; Schüller, W.; Britvin, S.N.; Pushcharovsky, D.Y. Betzite,  $\text{Na}_6\text{Ca}_2(\text{Al}_6\text{Si}_6\text{O}_{24})\text{Cl}_4$ , a new cancrinite-group mineral from the Eifel paleovolcanic region, Germany. *Can. J. Mineral. Petrol.* **2023**, *61*, 177–188. [[CrossRef](#)] [[PubMed](#)]
26. Bokiy, G.B.; Borutskiy, B.E. (Eds.) *Minerals. Vol. V(2): Framework Silicates*; Nauka: Moscow, Russia, 2003; 379p. (In Russian)
27. Leoni, L.; Mellini, M.; Merlino, S.; Orlandi, P. Cancrinite-like minerals: New data and crystal chemical considerations. *Rend. Della Soc. Ital. Mineral. Petrol.* **1979**, *35*, 713–719.
28. Hassan, I.; Buseck, P.R. The origin of the superstructure and modulations in cancrinite. *Can. Mineral.* **1992**, *30*, 49–59.
29. Rozenberg, K.A.; Rastsvetaeva, R.K.; Chukanov, N.V. Crystal structures of oxalate-bearing cancrinite with an unusual arrangement of  $\text{CO}_3$  groups and sulfate-rich davyne. *Crystallogr. Rep.* **2009**, *54*, 793–799. [[CrossRef](#)]
30. Bonaccorsi, E.; Merlino, S.; Pasero, M. Davyne from Zabargad (St. John's) Island: Peculiar chemical and structural features. *Acta Vulcanol.* **1991**, *2*, 55–63.
31. Eckert, B.; Steudel, F. Molecular spectra of sulfur molecules and solid sulfur allotropes. *Top. Curr. Chem.* **2003**, *231*, 31–97. [[CrossRef](#)]
32. Steudel, R. Inorganic polysulfides  $\text{S}_n^{2-}$  and radical anions  $\text{S}_n^{\bullet-}$ . In *Elemental Sulfur and Sulfur-Rich Compounds II. Topics in Current Chemistry*; Steudel, R., Ed.; Springer: Berlin/Heidelberg, Germany, 2003; Volume 231.
33. Steudel, R.; Chivers, T. The role of polysulfide dianions and radical anions in the chemical, physical and biological sciences, including sulfur-based batteries. *Chem. Soc. Rev.* **2019**, *48*, 3279–3319. [[CrossRef](#)]
34. Wong, M.W.; Steudel, R. Structure and spectra of tetrasulfur  $\text{S}_4$ —An ab initio MO study. *Chem. Phys. Lett.* **2003**, *379*, 162–169. [[CrossRef](#)]
35. Rigaku Oxford Diffraction. *CrysAlisPro Software System, Version 1.171.39.46*; Rigaku: Austin, TX, USA, 2018.
36. Finch, A.A.; Friis, H.; Maghrabi, M. Defects in sodalite-group minerals determined from X-ray-induced luminescence. *Phys. Chem. Miner.* **2016**, *43*, 481–491. [[CrossRef](#)]
37. Radomskaya, T.A.; Kaneva, E.V.; Shendrik, R.Y.; Suvorova, L.F.; Vladykin, N.V. Sulfur-bearing sodalite, hackmanite, in alkaline pegmatites of the Inagli massif (Aldan Shield): Crystal chemistry, photochromism, and luminescence. *Geol. Ore Depos.* **2021**, *63*, 696–704. [[CrossRef](#)]
38. Sheldrick, G.M. Crystal structure refinement with SHELXL. *Acta Cryst.* **2015**, *C71*, 3–8.
39. Pokrovski, G.S.; Dubrovinsky, L.S. The  $\text{S}_3^-$  ion is stable in geological fluids at elevated temperatures and pressures. *Science* **2011**, *331*, 1052–1054. [[CrossRef](#)]
40. Pokrovski, G.S.; Dubessy, J. Stability and abundance of the trisulfur radical ion  $\text{S}_3^-$  in hydrothermal fluids. *Earth Planet. Sci. Lett.* **2015**, *411*, 298–309. [[CrossRef](#)]
41. Chivers, T.; Elder, P.J.W. Ubiquitous trisulfur radical anion: Fundamentals and applications in materials science, electrochemistry, analytical chemistry and geochemistry. *Chem. Soc. Rev.* **2013**, *42*, 5996–6005. [[CrossRef](#)]
42. Chukanov, N.V.; Sapozhnikov, A.N.; Kaneva, E.V.; Varlamov, D.A.; Viskasina, M.F. Bystrite,  $\text{Na}_7\text{Ca}(\text{Al}_6\text{Si}_6\text{O}_{24})\text{S}_5^{2-}\text{Cl}^-$ : Formula redefinition and relationships with other four-layer cancrinite-group minerals. *Mineral. Mag.* **2023**, 1–29. [[CrossRef](#)]
43. Jacquemet, N.; Guillaume, D.; Zwicky, A.; Pokrovski, G.S. In situ Raman spectroscopy identification of the  $\text{S}_3^-$  ion in S-rich hydrothermal fluids from synthetic fluid inclusions. *Am. Mineral.* **2014**, *99*, 1109–1118. [[CrossRef](#)]
44. Waldner, P.; Pelton, A.D. Thermodynamic Modeling of the Fe-S System. *J. Phase Equilib. Diff.* **2005**, *26*, 23–28. [[CrossRef](#)]
45. Shishin, D.; Jak, E.; Decterov, A.A. Critical assessment and thermodynamic modeling of the Fe-O-S system. *J. Phase Equilib. Diffus.* **2015**, *36*, 224–240. [[CrossRef](#)]

46. Ivanov, V.G.; Sapozhnikov, A.N. *Lazurites of the USSR*; Nauka: Novosibirsk, Russia, 1985; 172p. (In Russian)
47. Drüppel, K.; Wagner, T.; Boyce, A.I. Evolution of sulfide mineralization in ferrocarnatite Swartbooisdrif, Northwestern Namibia: Constrains from mineral compositions and sulfur isotopes. *Can. Mineral.* **2006**, *44*, 877–894. [[CrossRef](#)]
48. Sapozhnikov, A.N.; Ivanov, V.G.; Levitsky, V.I.; Piskunova, L.F. Structural-mineralogical peculiarities of lazurite from SW Pamirs. *Zap. Vsesoyuznogo Mineral. Obs. (Proc. Mineral. Soc. USSR)* **1993**, *122*, 108–115. (In Russian)
49. Sapozhnikov, A.N.; Kaneva, E.V.; Cherepanov, D.I.; Suvorova, L.F.; Levitsky, V.I.; Ivanova, L.A.; Reznitsky, L.Z. Vladimirivanovite,  $\text{Na}_6\text{Ca}_2[\text{Al}_6\text{Si}_6\text{O}_{24}](\text{SO}_4, \text{S}_3, \text{S}_2, \text{Cl})_2 \cdot \text{H}_2\text{O}$ , a new mineral of sodalite group. *Geol. Ore Depos.* **2012**, *54*, 557–564. [[CrossRef](#)]
50. Kaneva, E.; Radomskaya, T.; Shendrik, R. Fluorcarletonite—A new blue gem material. *J. Gemmol.* **2022**, *38*, 376–785. [[CrossRef](#)]
51. Kaneva, E.; Bogdanov, A.; Radomskaya, T.; Belozerova, O.; Shendrik, R. Crystal-chemical characterization and spectroscopy of fluorcarletonite and carletonite. *Mineral. Mag.* **2023**, 1–13. [[CrossRef](#)]
52. Shendrik, R.; Kaneva, E.; Radomskaya, T.; Sharygin, I.; Marfin, A. Relationships between the structural, vibrational, and optical properties of microporous cancrinite. *Crystals* **2021**, *11*, 280. [[CrossRef](#)]
53. Kaneva, E.; Shendrik, R. Radiation defects and intrinsic luminescence of cancrinite. *J. Lumin.* **2022**, *243*, 118628. [[CrossRef](#)]
54. Henshaw, T.L.; Ongstad, A.P.; Lawconnell, R.I. Photodissociation of  $\text{S}_4\text{N}_4$ . I. 248 nm. *J. Chem. Phys.* **1992**, *96*, 53–66. [[CrossRef](#)]
55. Ogorodova, L.P.; Mel'chakova, L.V.; Vigasina, M.F.; Olysysh, L.V.; Pekov, I.V. Cancrinite and cancrisilite in the Khibina-Lovozero alkaline complex: Thermochemical and thermal data. *Geochem. Int.* **2009**, *47*, 260–267. [[CrossRef](#)]

**Disclaimer/Publisher's Note:** The statements, opinions and data contained in all publications are solely those of the individual author(s) and contributor(s) and not of MDPI and/or the editor(s). MDPI and/or the editor(s) disclaim responsibility for any injury to people or property resulting from any ideas, methods, instructions or products referred to in the content.